

Variational quantum metrology for multiparameter estimation under dephasing noise

Trung Kien Le,¹ Hung Q. Nguyen,² and Le Bin Ho^{3,4,*}

¹*Department of Physics, University of California, Santa Barbara, USA*

²*Nano and Energy Center, VNU University of Science, Vietnam National University, Hanoi*

³*Frontier Research Institute for Interdisciplinary Sciences, Tohoku University, Sendai 980-8578, Japan*

⁴*Department of Applied Physics, Graduate School of Engineering, Tohoku University, Sendai 980-8579, Japan*

We present a hybrid quantum-classical variational scheme to enhance precision in quantum metrology. In the scheme, both the initial state and the measurement basis in the quantum part are parameterized and optimized via the classical part. It enables the maximization of information gained about the measured quantity. We discuss specific applications to 3D magnetic field sensing under several dephasing noise modes. Indeed, we demonstrate its ability to simultaneously estimate all parameters and surpass the standard quantum limit, making it a powerful tool for metrological applications.

I. INTRODUCTION

Quantum metrology is an estimation process that utilizes unique quantum phenomena such as entanglement and squeezing to improve the precision of estimation beyond classical limits [1–3]. Recent development in quantum computing leads to numerous optimal algorithms for enhancing precision in single-parameter estimation, such as adaptive measurements [4–7], quantum error correction [8, 9], and optimal quantum control [10–12]. So far, a variational algorithm has been demonstrated by combining the advantages of both quantum and classical systems for quantum-enhanced metrology [12–15]. A similar protocol for spin systems was also introduced [16, 17].

Multiparameter estimation is essential in various fields, such as Hamiltonian tomography [18], multiphase sensing [19–21], gravitational wave detection [22], and atomic clocks [23, 24]. However, the estimation is more challenging due to the incompatibility [25]. In these cases, simultaneous determination of all parameters is impossible, resulting in a tradeoff [26]. Numerous techniques have been introduced to tackle this challenge, including establishing optimal measurement strategies [27, 28], employing parallel scheme [21], sequential feedback scheme [29], and implementing post-selection procedures [30]. More recently, a variational toolbox for multiparameter estimation was proposed [31], which is a generalization from the previous work mentioned above [14].

While using variational schemes is promising, their potential significance in multiparameter quantum metrology has yet to be fully understood, even in principle. Furthermore, determining the optimal quantum resources and measurement strategy to extract maximum information about all parameters is limited by the tradeoffs in estimating incompatible observables [26, 32, 33] and required collective measurements over multiple copies of a probe state [32, 33]. Therefore, finding a suitable and practical strategy for precise estimation of multiple parameters remains a thriving area of quantum metrology.

In this work, we propose a variational scheme to enhance the precision of multiparameter estimation in the presence of dephasing noise. The basic idea is to use a quantum computer to prepare a trial state (an ansatz) that depends on a set of trainable variables. The state is subjected to a series of control operations, representing unknown multiparameter and noise, and then is measured through observables determined by other trainable variables. The measurement results are used to update the trainable variables and optimize the estimation of the unknown parameters.

Optimizing both the initial probe state and the measurement operators allows us to identify suitable conditions for the quantum probe to increase sensitivity and achieve the ultimate quantum limit for all parameters. In numerical simulations, we estimate a 3D magnetic field under a dephasing noise model and find that sensitivity for all parameters can simultaneously reach the ultimate quantum bound, i.e., the classical bound equals the quantum bound. We also examine a time-dependent Ornstein-Uhlenbeck model [34] and observe results surpassing the standard quantum limit by increasing the probe's number of particles. This approach holds promise for a wide range of metrological applications, including external field sensing, precision spectroscopy, gravitational wave detection, and others, where the effects of noises cannot be ignored.

II. RESULTS

A. Variational quantum metrology

The goal of multiparameter estimation is to evaluate a set of unknown d parameters $\phi = (\phi_1, \phi_2, \dots, \phi_d)^\top$, which are imprinted onto a quantum probe via a unitary evolution $U(\phi) = \exp(-it\mathbf{H}\phi) = \exp(-it\sum_{k=1}^d H_k\phi_k)$, where $\mathbf{H} = (H_1, H_2, \dots, H_d)$ are non-commuting Hermitian Hamiltonians. The precision of estimated parameters $\check{\phi}$ is evaluated using a mean square error matrix (MSEM) $V = \sum_m p(m|\phi) [\check{\phi}(m) - \phi] [\check{\phi}(m) - \phi]^\top$, where $p(m|\phi) = \text{Tr}[\rho(\phi)E_m]$ is the probability for obtaining an outcome m when measuring the final state $\rho(\phi)$ by an element E_m in a

*Electronic address: binho@fris.tohoku.ac.jp

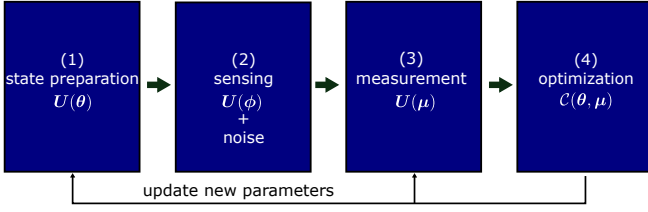


FIG. 1: **Variational quantum metrology.** (1) use quantum circuit $U(\theta)$ to prepare a variational state; (2) encode multiparameter ϕ and noise using $U(\phi)$ and noise channels; (3) use circuit $U(\mu)$ to create a variational POVM for measurement; (4) send measurement results to a classical computer to optimize cost function $\mathcal{C}(\theta, \mu)$ using a gradient-based optimizer. Update new training variables and repeat the scheme until it converges.

positive, operator-value measure (POVM). For unbiased estimators, the MSEM obeys the Cramér-Rao bounds (CRBs) [35–38]

$$\text{Tr}[WV] \geq C_F \geq C_{\text{NH}} \geq C_H \geq C_S, \quad (1)$$

where W is a scalar weight matrix, which can be chosen as an identity matrix without loss of generality. The classical bound is $C_F = \text{Tr}[WF^{-1}]$, where F is the classical Fisher information matrix (CFIM) with elements $F_{ij} = \sum_m \frac{1}{p(m|\phi)} [\partial_{\phi_i} p(m|\phi)] [\partial_{\phi_j} p(m|\phi)]$ [39]. The Nagaoka–Hayashi bound C_{NH} and Holevo bound C_H are given via semidefinite programming, i.e., $C_{\text{NH}} = \min_{\{D, X\}} \text{Tr}[(W \otimes \rho(\phi)) \cdot D]$ [38, 40], and $C_H = \min_{\{X\}} (\text{Tr}[W \text{Re}Z + \|\sqrt{W} \text{Im}Z \sqrt{W}\|])$ [36, 41], where D is a d -by- d matrix contains Hermitian operators D_{ij} and satisfies $D \geq XX^\dagger$, $X = (X_1, X_2, \dots, X_d)^\dagger$ satisfies $\text{Tr}[\rho(\phi) X_j] = \phi_j$ and $\text{Tr}[X_i \partial_{\phi_j} \rho(\phi)] = \delta_{ij}$, Z is a positive semidefinite matrix with elements $Z_{ij} = \text{Tr}[X_i X_j \rho(\phi)]$. Finally, $C_S = \text{Tr}[WQ^{-1}]$ is a symmetric logarithmic derivative (SLD) quantum bound where $Q_{ij} = \text{Re}[\text{Tr}[\rho(\phi) L_i L_j]]$ is the real symmetric quantum Fisher information matrix (QFIM) that defined through the SLD $2\partial_{\phi_j} \rho(\phi) = \{L_j, \rho(\phi)\}$ [39].

Although optimal estimators can achieve C_F [42], the C_{NH} can be attained with separable measurements for qubits probes [40], and asymptotic achievement of C_H is possible [43–47], it is not always possible to attain C_S for multiparameter estimation [41]. In this work, we attempt to reach this bound. In some instances, $C_H = C_S$ if a weak commutativity condition $\text{Im}(\text{Tr}[L_j L_i \rho(\phi)]) = 0$ is met [41, 48]. A similar condition for pure states is also applied to attain $C_F = C_S$ [19, 49, 50]. Further discussion on the interplay between C_{NH} , C_H , and C_S has been reported [37]. However, this condition alone is insufficient to achieve the quantum bounds practically; instead, attaining C_S and C_H also requires entangled measurements (POVM) over multiple copies [45, 46]. Recently, Yang et al., have derived saturation conditions for general POVMs [28]. To be more precise, when $F \geq Q > 0$ and for any arbitrary full-rank positive weight matrix $W > 0$, the equally $C_F = C_S$ implies $F = Q$.

This paper presents a variational quantum metrology (VQM) scheme following Meyer et al. toolbox [31] as sketched in Fig. 1 to optimize both the preparation state and POVM. A

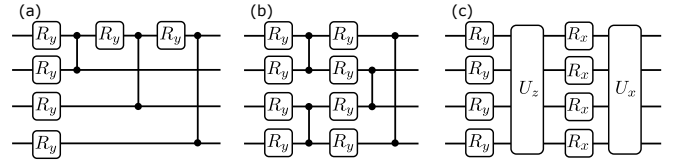


FIG. 2: **Ansatzes for preparation state and POVM.** (a) star topology entangled ansatz. (b) ring topology entangled ansatz. (c) squeezing ansatz. In the circuits, $R_{x(y)}$: x (y)-rotation gate, $U_{x(z)}$: global Mølmer–Sørensen gate, $\bullet\text{---}\bullet$: controlled-Z gate.

quantum circuit $U(\theta)$ is used to generate a variational preparation state with trainable variables θ . Similar quantum circuit with variables μ is used to generate a variational POVM $E(\mu) = \{E_m(\mu) = U^\dagger(\mu) E_m U(\mu) > 0 | \sum_m E_m(\mu) = I\}$. Using classical computers, a cost function $\mathcal{C}(\theta, \mu)$ can be optimized to update the variables for quantum circuits, resulting in enhanced information extraction. The scheme is repeated until it converges.

To investigate the attainable the ultimate SLD quantum bound, we define the cost function by a relative difference [47]

$$\mathcal{C}(\theta, \mu) = 1 - \frac{C_S}{C_F}, \quad (2)$$

which is positive semidefinite according to Eq. (1). The variables are trained by solving the optimization task $\arg \min_{\{\theta, \mu\}} \mathcal{C}(\theta, \mu)$. As the value of $\mathcal{C}(\theta, \mu)$ approaches zero, we reach the ultimate SLD quantum bound where $C_F = C_S$. Notably, we strive for agreement between classical and SLD quantum bounds assuming $\text{Tr}[WV] = C_F$, and thus, omit discussion on the estimator for achieving $\text{Tr}[WV] = C_F$. Moreover, the cost function (2) serves as a technical tool to optimize the variational scheme, while the main analyzing quantities are CRBs. A vital feature of the VQM is using variational quantum circuits, which allows for optimizing the entangled probe state and measurements to extract the maximum information about the estimated parameters. This approach thus does not require entangled measurements over multiple copies. We further discuss various cost functions in the Discussion section.

B. Ansatzes

We propose three variational circuits: a star topology ansatz, a ring topology ansatz, and a squeezing ansatz. The first two ansatzes are inspired by quantum graph states, which are useful resources for quantum metrology [51, 52]. A conventional graph state is formed by a collection of vertices V and edges D as $G(V, D) = \prod_{i,j \in D} CZ^{ij} |+\rangle^V$, where CZ^{ij} represents the controlled-Z gate connecting the i and j qubits, and $|+\rangle$ is an element in the basis of Pauli σ_x . The proposed ansatzes here incorporate y -rotation gates ($R_y(\theta) = e^{-i\theta \sigma_y/2}$) at every vertex prior to CZ gates (see Fig. 2a,b). The squeezing ansatz in Fig. 2c is inspired by squeezing states, which is another useful resource for quantum metrology [53–55]. It has x (y)-rotation gates and global Mølmer–Sørensen gates $U_{x(z)}$, where

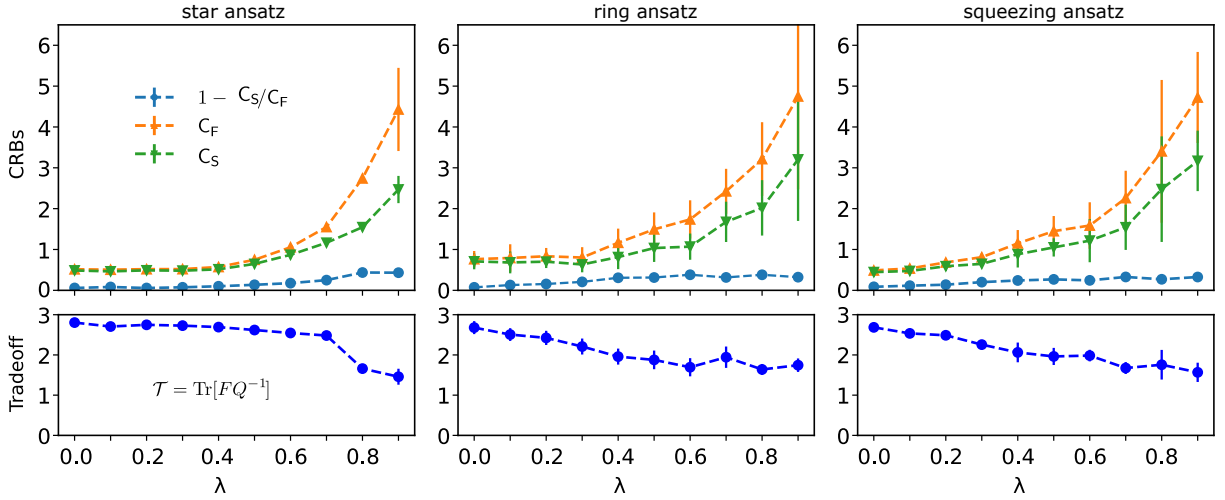


FIG. 3: **Variational quantum metrology under dephasing noise.** (Top): plot of the optimal cost function $\mathcal{C}(\boldsymbol{\theta}, \boldsymbol{\mu})$, classical bound C_F , and SLD quantum bound C_S as functions of dephasing probability. From left to right: star, ring, and squeezing ansatz. (Bottom): plot of corresponding tradeoff \mathcal{T} . Numerical results are calculated at $N = 3$, the optimal number of layers in Fig. 8, and the results are averaged after 10 samples.

$U_{x(z)} = \exp(-i \sum_{j=1}^N \sum_{k=j+1}^N \sigma_{x(z)} \otimes \sigma_{x(z)} \frac{\chi_{jk}}{2})$ for an N -qubit circuit [56]. The trainable variables for one layer are $2N - 2$, $2N$, and $N(N + 1)$ for the star, ring, and squeezing ansatz, respectively. Hereafter, we use these ansatzes for generating variational preparation states and variational POVM in the VQM scheme.

C. Multiparameter estimation under dephasing noise

After preparing a variational state $\rho(\boldsymbol{\theta}) = \mathbf{U}(\boldsymbol{\theta})\rho_0\mathbf{U}(\boldsymbol{\theta})$, we use it to estimate a 3D magnetic field under dephasing noise. The field is imprinted onto every single qubit via the Hamiltonian $\mathbf{H} = \sum_{i \in \{x, y, z\}} \phi_i \sigma_i$, where $\boldsymbol{\phi} = (\phi_x, \phi_y, \phi_z)$, and σ_i is a Pauli matrix. Under dephasing noise, the variational state $\rho(\boldsymbol{\theta})$ evolves to [57]

$$\mathcal{E}_t(\rho) = \left[\prod_{k=1}^N e^{\gamma t \mathcal{L}^{(k)}} \right] e^{-it\mathcal{H}} \rho, \quad (3)$$

where we omitted $\boldsymbol{\theta}$ in $\rho(\boldsymbol{\theta})$ for short. The superoperator \mathcal{H} generates a unitary dynamic $\mathcal{H}\rho = [\mathbf{H}, \rho]$, and $\mathcal{L}^{(k)}$ is a non-unitary dephasing superoperator with γ is the decay rate. In terms of Kraus operators, the dephasing superoperator gives

$$e^{\gamma t \mathcal{L}^{(k)}} \rho = K_1^{(k)} \rho [K_1^{(k)}]^\dagger + K_2^{(k)} \rho [K_2^{(k)}]^\dagger, \quad (4)$$

where $K_1 = \begin{pmatrix} \sqrt{1-\lambda} & 0 \\ 0 & 1 \end{pmatrix}$ and $K_2 = \begin{pmatrix} \sqrt{\lambda} & 0 \\ 0 & 0 \end{pmatrix}$ are Kraus operators, and $\lambda = 1 - e^{-\gamma t}$ is the dephasing probability. Finally, the state is measured in the variational POVM $\mathbf{E}(\boldsymbol{\mu})$ and yields the probability $p(m) = \text{Tr}[\mathcal{E}_t(\rho) E_m(\boldsymbol{\mu})]$. Note that p also depends on $\boldsymbol{\theta}$, $\boldsymbol{\phi}$, and $\boldsymbol{\mu}$.

It is important to attain the ultimate SLD quantum bound, i.e., $C_F = C_S$. We thus compare numerical results for the cost

function, C_F , and C_S as shown in the top panels of Fig. 3. At each λ , the cost function and other quantities are plotted with the optimal $\boldsymbol{\theta}$ obtained after stopping the training by EarlyStopping callback [58]. The numerical results are presented at $N = 3$, and the number of layers is chosen from their optimal values as shown in the Method and Fig. 8. Through the paper, we fixed $(\phi_x, \phi_y, \phi_z) = (\pi/6, \pi/6, \pi/6)$.

We find that for small noises, C_F reaches C_S , which is consistent with earlier numerical findings [46, 47]. Remarkably, different from the previous findings where the convergence of these bounds is not clear, here we show that both C_F and C_S remain small (also in comparison to previous work [31]) without any divergence. We further compare the performance of the star ansatz to that of the ring and squeezing ansatzes. It saturates the ultimate quantum limit for dephasing probabilities $\lambda < 0.5$, whereas the ring and squeezing ansatzes only reach the limit for $\lambda < 0.2$. The reason is that the star graph exhibits a central vertex connected to the remaining $N - 1$ surrounding vertices, which facilitates robust quantum metrology, as discussed in [51].

Furthermore, we evaluate the tradeoff between the CFIM and QFIM by introducing a function $\mathcal{T} = \text{Tr}[FQ^{-1}]$. For unknown d parameters, the naive bound is $\max(\mathcal{T}) = d$, leading to simultaneous optimization of all parameters. The results are shown in the bottom panels of Fig. 3 and agree well with the CRBs presented in the top panels, wherein $\mathcal{T} \rightarrow 3$ whenever the SLD quantum bound is reached. So far, we observe that $\mathcal{T} > d/2$ for all cases, which is better than the theoretical prediction previously [59]. This observation exhibits a practical advantage of the VQM approach across different levels of noise.

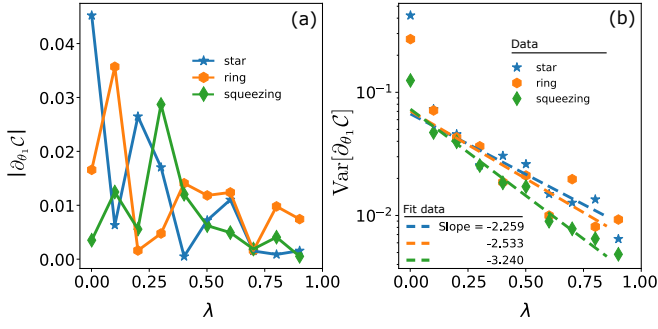


FIG. 4: **Barren plateau.** (a) Plot of $|\partial_{\theta_1} C|$ as a function of the dephasing probability λ . (b) Plot of the variance of gradient $\text{Var}[\partial_{\theta_1} C]$. The slope of each fit line indicates the exponential decay of the gradient, which is a sign of the barren plateau effect. The results are taken average after 200 runs.

D. Barren Plateaus

Variational quantum circuits under the influence of noises will exhibit a barren plateau (BP), where the gradient along any direction of the variables' space vanishes exponentially with respect to the noise level [60]. The BP prevents reaching the global optimization of the training space, thereby reducing the efficiency and trainability of the variational quantum circuit. However, BPs can be partially mitigated through carefully designing ansatzes and cost functions [61].

The deviation of CRBs shown in Fig. 3 may be subject to the BP raised by noise. We examine such dependent and show the results in Fig. 4. We plot $|\partial_{\theta_1} C|$ (Fig. 4a) and $\text{Var}[\partial_{\theta_1} C]$ (Fig. 4b), where C is defined in Eq. (2) after 200 runs with random initialization of θ and μ for each value of λ . As predicted, both of them demonstrate an exponential decline with an increase in the dephasing probability. Especially, $\text{Var}[\partial_{\theta_1} C]$ exponentially vanishes with the slope of -2.259, -2.533, and -3.240 for the star, ring, and squeezing ansatz, respectively. The star ansatz exhibits slower gradient decay as λ approaches 1 due to its smaller trainable variables' space than the ring and squeezing ansatz. This indicates better training and less susceptibility to vanishing gradients, leading to better achievement of the ultimate quantum bound.

E. Multiparameter estimation under the Ornstein-Uhlenbeck model

We consider the Ornstein-Uhlenbeck model, where the noise is induced by the stochastic fluctuation of the external (magnetic) field [34]. The Kraus operators are [62]

$$K_1(t) = \begin{pmatrix} \sqrt{1-q(t)} & 0 \\ 0 & 1 \end{pmatrix}, K_2(t) = \begin{pmatrix} \sqrt{q(t)} & 0 \\ 0 & 0 \end{pmatrix}, \quad (5)$$

where $q(t) = 1 - e^{-f(t)}$ with $f(t) = \gamma[t + \tau_c(e^{-t/\tau_c} - 1)]$, and τ_c represents the memory time of the environment. In the Markovian limit ($\tau_c \rightarrow 0$), $f(t) = \gamma t$, which corresponds to the previous dephasing case. In the non-Markovian limit

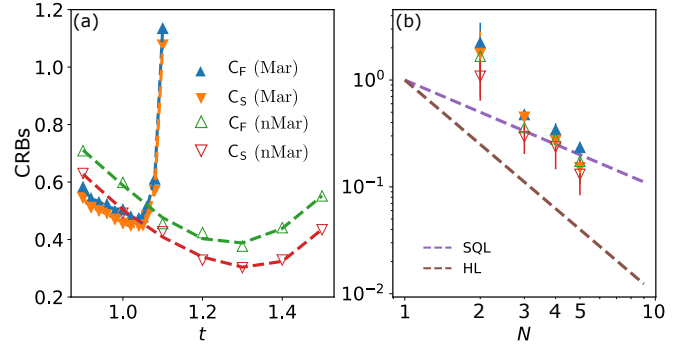


FIG. 5: **Variational quantum metrology under time-dephasing noise.** (a): we present the CRBs as functions of the sensing time, demonstrating an optimal sensing time for achieving each minimum CRB. The non-Markovian dephasing (nMar) produces lower metrological bounds in comparison to the Markovian one (Mar). (b): plot of the minimal bounds for cases in (a), comparing them with the standard quantum limit (SQL) and the Heisenberg limit (HL). For non-Markovian metrology, the bounds surpass the SQL, as predicted.

with large τ_c , such as $t/\tau_c \ll 1$, we have $f(t) = \frac{\gamma t^2}{2\tau_c}$. In the numerical simulation, we fixed $\gamma = 0.1$ and $\tau_c = 20$ (for non-Markovian)

$$q(t) = \begin{cases} 1 - \exp(-0.1t) & \text{Markovian,} \\ 1 - \exp(-\frac{t^2}{400}) & \text{non-Markovian.} \end{cases} \quad (6)$$

We use this model to study the relationship between sensing time, Markovianity, and ultimate attainability of the quantum bound. Figure 5a displays the optimal CRBs for Markovian and non-Markovian noises as functions of sensing time t . As previously reported in [20], there exists an optimal sensing time that minimizes the CRBs for each case examined here. Moreover, the non-Markovian dephasing (nMar) results in lower metrological bounds as compared to the Markovian case (Mar). So far, the minimum CRBs for different N are presented in Figure 5b. The results demonstrate that with an increase in N , the non-Markovian noise attains a better bound than the standard quantum limit (SQL) for both classical and SLD quantum bounds. This observation agrees with previous results reported using semidefinite programming [63], indicating the potential of variational optimization for designing optimal non-Markovian metrology experiments. Finally, we note that in the Ornstein-Uhlenbeck model, the SLD quantum bound is unachievable, as indicated by $C_F > C_S$. It remains a question for future research on whether one can attain the SLD quantum bound with probe designs, and the existence of tight bounds in the non-Markovian scenario.

III. DISCUSSION

A. Concentratable entanglement

We discuss how the three ansatzes create entangled states and the role of entangled resources in achieving the SLD quan-

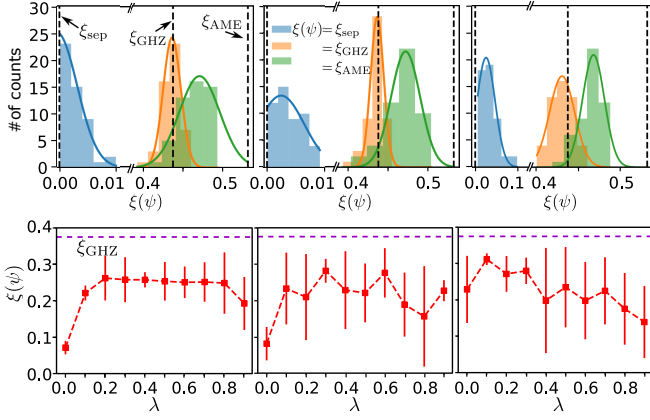


FIG. 6: **Entanglement generation.** (Top): from left to right: the distribution of training CEs corresponds to the star, ring, and squeezing ansatzes, respectively. All the ansatzes can produce separable and GHZ states, but generating an AME state is challenging. The results are shown at $N = 4$ and (2-2) layers for each ansatz. (Bottom): the CEs are plotted at the optimal CRBs in Fig. 3, using the same circuit setup that in the figure. Again, λ is the dephasing probability.

tum bound in VQM. We analyze entanglement using the concentratable entanglement (CE) defined by [64]

$$\xi(\psi) = 1 - \frac{1}{2^{|s|}} \sum_{\alpha \in \mathcal{P}(s)} \text{Tr}[\rho_\alpha^2], \quad (7)$$

where $\mathcal{P}(s)$ is the power set of s , $\forall s \in \{1, 2, \dots, N\}$, and ρ_α is the reduced state of $|\psi\rangle$ in the subsystem α with $\rho_\theta := I$. Practically, $\xi(\psi)$ can be computed using the SWAP test circuit as stated in Ref. [64], where $\xi(\psi) = 1 - p(\mathbf{0})$, with $p(\mathbf{0})$ is the probability of obtaining $|00 \dots 0\rangle$. The ability of the SWAP test to compute CE is due to the equivalence between conditional probability distribution and the definition of CE.

We first train the three ansatzes to evaluate their ability of entangled-state generation. Particularly, the training process aims to generate quantum states with $\xi(\psi) = \{\xi_{\text{sep}}, \xi_{\text{GHZ}}, \xi_{\text{AME}}\}$, where $\xi_{\text{sep}} = 0$ for a separable state, $\xi_{\text{GHZ}} = \frac{1}{2} - \frac{1}{2^N}$ for a GHZ state, and $\xi_{\text{AME}} = 1 - \frac{1}{2^N} \sum_{j=0}^N \binom{N}{j} \frac{1}{2^{\min(j, N-j)}}$ for an absolutely maximally entangled (AME) state [65, 66]. The top panels in Fig. 6 display the results for star, ring, and squeezing ansatz, from left to right, at $N = 4$ and (2-2) layers of each ansatz as an example. All the ansatzes examined can reach the separable and GHZ state, but hard to achieve the AME state. This observation is consistent with the CEs for conventional graph states [66].

We next discuss the role of entanglement in achieving the ultimate SLD quantum bound. In the bottom panels of Fig. 6, we graph the corresponding CEs at the optimal CRBs shown in Fig. 3, which apparently do not require the maximum entanglement (e.g., GHZ) to achieve the ultimate SLD quantum bound. This phenomenon can be explained by the fact that maximum entanglement is not required for high-precision quantum metrology, as previously noted in Refs. [67–69]. Therefore, emphasizing the robustness of easily preparable entangled probe states and non-local POVM schemes would be

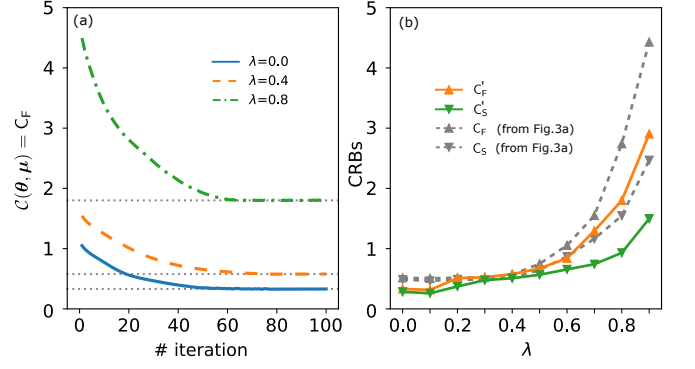


FIG. 7: Optimizing classical bound C_F through Variational Quantum Metrology. (a): Plot of the cost function $\mathcal{C}(\theta, \mu) = C_F$ versus the number of iterations across various noise probabilities λ . (b) Plot of the corresponding optimal values of C'_F and C'_S , and their counterparts extracted from Figure 3a (in grayscale). These numerical results pertain to the star-graph configuration.

advantageous for quantum metrological applications exposed to Markovian and non-Markovian noises.

B. Cost functions

We address the selection of the cost function used in the variational algorithm. The preference outlined in Eq. (2) is not the sole option. An alternative approach could involve adopting the classical bound C_F as the cost function to maximize the information extraction. However, this way does not guarantee the classical bound can reach the quantum bound, a requirement in estimation theory. In Figure 7a, we present a plot depicting the cost function $\mathcal{C}(\theta, \mu) = C_F$ as a function of the number of iterations, considering various noise probabilities λ . It demonstrates that the cost function reaches its minimum value at a certain iteration. Correspondingly, in Figure 7b, we provide the optimal values for both classical and quantum bounds, denoted as C'_F and C'_S , alongside this optimization. It's important to emphasize that this approach does not guarantee that C'_F equals C'_S . For comparison, we include a grayscale representation of these quantities, originally presented in Figure 3a. Here, optimizing the cost function Eq.(2) still ensures small values and convergence for both C_F and C_S . However, C'_F and C'_S consistently remain below C_F and C_S . This behavior occurs because the evaluation of C_F and C_S is based on the state that maximizes the figure of merit in Eq. (2), rather than solely minimizing C_F or C_S .

Furthermore, alternative physical quantities, such as the tradeoff \mathcal{T} and the norm-2, can also be utilized as potential cost functions. For instance, a tradeoff cost function is analogous to the one presented in Eq. (2), taking the form:

$$\mathcal{C}(\theta, \mu) = 1 - \frac{1}{d} \text{Tr}[FQ^{-1}], \quad (8)$$

where d is the number of estimated parameters. Notably, in scenarios where Q is a diagonal matrix and $\mathcal{C}(\theta, \mu) = 0$, it results in a zero tradeoff, i.e., $\frac{F_{11}}{Q_{11}} = \dots = \frac{F_{dd}}{Q_{dd}} = 1$.

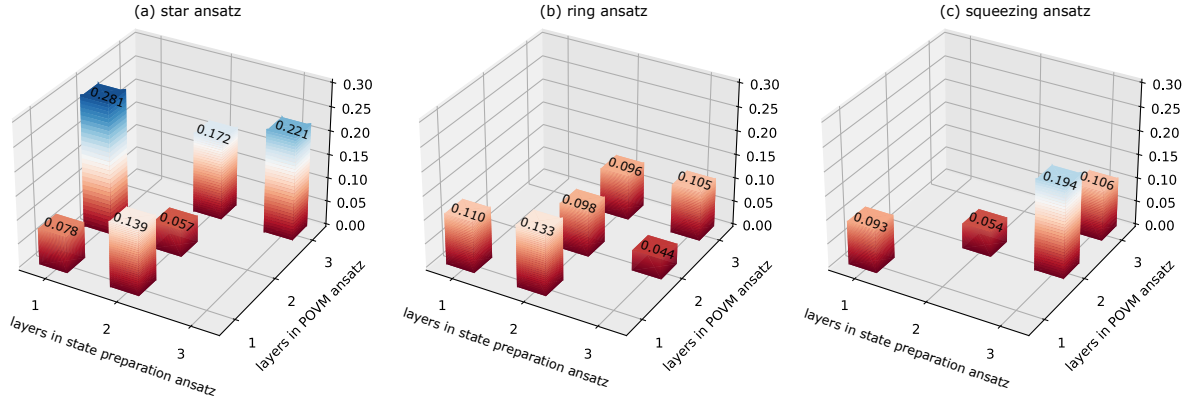


FIG. 8: **Cost function vs the optimal number of layers for different ansatzes.** The plot of the cost function for (a) star ansatz, (b) ring ansatz, and (c) squeezing ansatz at $N = 3$ without noise. The minimum cost function vs the number of layers are (0.057, 2-2), (0.044, 3-2), and (0.054, 2-2), respectively.

Additionally, norm-2 can also function as a viable cost function [27].

$$\mathcal{C}(\theta, \mu) = \|F - Q\|_2, \quad (9)$$

where $\|A\|_2 = \sqrt{\lambda_{\max}(A^*A)}$ represents the norm-2, with λ_{\max} is the maximum eigenvalue. However, it is worth noting that these alternate cost functions might not be convex nor trainable [61]. As a result, the selection of the cost function in Eq. (2) is indeed appropriate.

IV. METHODS

A. Quantum circuit training

In numerical simulations, we employ the ADAM optimizer to train the VQM variables [70], where the variables at step $k + 1$ are given by

$$\theta^{k+1} = \theta^k - \alpha \frac{\hat{m}_k}{\sqrt{\hat{v}_k} + \epsilon}, \quad (10)$$

where $m_k = \beta_1 m_{k-1} + (1 - \beta_1) \nabla_{\theta} \mathcal{C}(\theta)$, $v_k = \beta_2 v_{k-1} + (1 - \beta_2) \nabla_{\theta}^2 \mathcal{C}(\theta)$, $\hat{m}_k = m_k / (1 - \beta_1^k)$, $\hat{v}_k = v_k / (1 - \beta_2^k)$, with the hyper-parameters are chosen as $\alpha = 0.2$, $\beta_1 = 0.8$, $\beta_2 = 0.999$ and $\epsilon = 10^{-8}$. The gradient $\partial_{\theta_i} \mathcal{C}(\theta)$ is given through the parameter-shift rule [71, 72]. The simulations are performed in Qiskit Aer simulator [73]. The number of iterations is chosen using the EarlyStopping callback [58].

To determine the appropriate number of layers for the preparation state and POVM ansatzes, we analyze the cost function (2) with different number of layers. We use $(\star, \dagger, \ddagger)$ to denote the minimum cost function, the number of layers for variational state preparation, and the number of layers for variational POVM. The results are shown in Fig. 8 with $(\star, \dagger, \ddagger) =$

(0.057, 2-2), (0.04, 3-2), and (0.054, 2-2) for the star, ring, and squeezing ansatz, respectively. Obviously, the metrological performances of these ansatzes demonstrate that deep ansatzes are unnecessary, as also noted in [46] where a shallow ansatz was able to saturate quantum bound. For the numerical simulations presented in this paper, we keep the number of layers fixed at these values.

B. Computing Fisher information

Classical and quantum Fisher information matrices can be computed in quantum circuits using the finite difference approximation. For the CFIM, we first derive an output probability as $\partial_{\phi_i} p = \frac{p(\phi_i+s) - p(\phi_i-s)}{2s}$, for a small shift s . We then compute the CFIM from $F_{ij} = \sum_m \frac{1}{p(m|\phi)} [\partial_{\phi_i} p(m|\phi)] [\partial_{\phi_j} p(m|\phi)]$. For the QFIM, we explicitly derive $Q_{ij} = 2 \text{vec}[\partial_{\phi_i} \rho(\phi)]^\dagger [\rho(\phi)^* \otimes I + I \otimes \rho(\phi)]^\dagger \text{vec}[\partial_{\phi_j} \rho(\phi)]$, where $\text{vec}[\cdot]$ is the vectorization of a matrix, and the superscript ‘+’ denotes the pseudo-inversion [74]. Again, we apply the finite difference to compute $\partial_{\phi_i} \rho = \frac{\rho(\phi_i+s) - \rho(\phi_i-s)}{2s}$, and substitute into the above equations to compute the QFIM.

All codes used to produce the findings of this study are incorporated into tqix [75, 76] and available at: <https://github.com/echkon/tqix-developers>. See also the Supplementary Material for tutorial codes.

Acknowledgments

We thank C.Q. Nguyen for assisting with the initial code. This work is supported by JSPS KAKENHI Grant Number 23K13025.

[1] Samuel L. Braunstein and Carlton M. Caves. Statistical distance and the geometry of quantum states. *Phys. Rev. Lett.*, 72:3439–

- [2] Vittorio Giovannetti, Seth Lloyd, and Lorenzo Maccone. Advances in quantum metrology. *Nature Photonics*, 5(4):222–229, Apr 2011.
- [3] Géza Tóth and Iagoba Apellaniz. Quantum metrology from a quantum information science perspective. *Journal of Physics A: Mathematical and Theoretical*, 47(42):424006, oct 2014.
- [4] O E Barndorff-Nielsen and R D Gill. Fisher information in quantum statistics. *Journal of Physics A: Mathematical and General*, 33(24):4481, jun 2000.
- [5] Akio Fujiwara. Strong consistency and asymptotic efficiency for adaptive quantum estimation problems. *Journal of Physics A: Mathematical and General*, 39(40):12489, sep 2006.
- [6] Yi-Hao Zhang and Wen Yang. Improving spin-based noise sensing by adaptive measurements. *New Journal of Physics*, 20(9):093011, sep 2018.
- [7] Rafał Demkowicz-Dobrzański, Jan Czajkowski, and Pavel Sekatski. Adaptive quantum metrology under general markovian noise. *Phys. Rev. X*, 7:041009, Oct 2017.
- [8] E. M. Kessler, I. Lovchinsky, A. O. Sushkov, and M. D. Lukin. Quantum error correction for metrology. *Phys. Rev. Lett.*, 112:150802, Apr 2014.
- [9] Sisi Zhou, Mengzhen Zhang, John Preskill, and Liang Jiang. Achieving the heisenberg limit in quantum metrology using quantum error correction. *Nature Communications*, 9(1):78, Jan 2018.
- [10] Jing Yang, Shengshi Pang, Zekai Chen, Andrew N. Jordan, and Adolfo del Campo. Variational principle for optimal quantum controls in quantum metrology. *Phys. Rev. Lett.*, 128:160505, Apr 2022.
- [11] Shengshi Pang and Andrew N. Jordan. Optimal adaptive control for quantum metrology with time-dependent hamiltonians. *Nature Communications*, 8(1):14695, Mar 2017.
- [12] Xiaodong Yang, Xi Chen, Jun Li, Xinhua Peng, and Raymond Laflamme. Hybrid quantum-classical approach to enhanced quantum metrology. *Scientific Reports*, 11(1):672, Jan 2021.
- [13] Bálint Koczor, Suguru Endo, Tyson Jones, Yuichiro Matsuzaki, and Simon C Benjamin. Variational-state quantum metrology. *New Journal of Physics*, 22(8):083038, aug 2020.
- [14] Ziqi Ma, Pranav Gokhale, Tian-Xing Zheng, Sisi Zhou, Xiaofei Yu, Liang Jiang, Peter Maurer, and Frederic T. Chong. Adaptive circuit learning for quantum metrology. In *2021 IEEE International Conference on Quantum Computing and Engineering (QCE)*, pages 419–430, 2021.
- [15] Raphael Kaubruegger, Pietro Silvi, Christian Kokail, Rick van Bijnen, Ana Maria Rey, Jun Ye, Adam M. Kaufman, and Peter Zoller. Variational spin-squeezing algorithms on programmable quantum sensors. *Phys. Rev. Lett.*, 123:260505, Dec 2019.
- [16] Raphael Kaubruegger, Denis V. Vasilyev, Marius Schulte, Klemens Hammerer, and Peter Zoller. Quantum variational optimization of ramsey interferometry and atomic clocks. *Phys. Rev. X*, 11:041045, Dec 2021.
- [17] Tian-Xing Zheng, Anran Li, Jude Rosen, Sisi Zhou, Martin Koppenhöfer, Ziqi Ma, Frederic T. Chong, Aashish A. Clerk, Liang Jiang, and Peter C. Maurer. Preparation of metrological states in dipolar-interacting spin systems. *npj Quantum Information*, 8(1):150, Dec 2022.
- [18] Zhi Li, Liujun Zou, and Timothy H. Hsieh. Hamiltonian tomography via quantum quench. *Phys. Rev. Lett.*, 124:160502, Apr 2020.
- [19] Tillmann Baumgratz and Animesh Datta. Quantum enhanced estimation of a multidimensional field. *Phys. Rev. Lett.*, 116:030801, Jan 2016.
- [20] Le Bin Ho, Hideaki Hakoshima, Yuichiro Matsuzaki, Masayuki Matsuzaki, and Yasushi Kondo. Multiparameter quantum estimation under dephasing noise. *Phys. Rev. A*, 102:022602, Aug 2020.
- [21] Zhibo Hou, Zhao Zhang, Guo-Yong Xiang, Chuan-Feng Li, Guang-Can Guo, Hongzhen Chen, Liqiang Liu, and Haidong Yuan. Minimal tradeoff and ultimate precision limit of multiparameter quantum magnetometry under the parallel scheme. *Phys. Rev. Lett.*, 125:020501, Jul 2020.
- [22] Roman Schnabel, Nergis Mavalvala, David E. McClelland, and Ping K. Lam. Quantum metrology for gravitational wave astronomy. *Nature Communications*, 1(1):121, Nov 2010.
- [23] Andrei Derevianko and Hidetoshi Katori. Colloquium: Physics of optical lattice clocks. *Rev. Mod. Phys.*, 83:331–347, May 2011.
- [24] Andrew D. Ludlow, Martin M. Boyd, Jun Ye, E. Peik, and P. O. Schmidt. Optical atomic clocks. *Rev. Mod. Phys.*, 87:637–701, Jun 2015.
- [25] Francesco Albarelli and Rafał Demkowicz-Dobrzański. Probe incompatibility in multiparameter noisy quantum metrology. *Phys. Rev. X*, 12:011039, Mar 2022.
- [26] Ilya Kull, Philippe Allard Guérin, and Frank Verstraete. Uncertainty and trade-offs in quantum multiparameter estimation. *Journal of Physics A: Mathematical and Theoretical*, 53(24):244001, may 2020.
- [27] Luca Pezzè, Mario A. Ciampini, Nicolò Spagnolo, Peter C. Humphreys, Animesh Datta, Ian A. Walmsley, Marco Barbieri, Fabio Sciarrino, and Augusto Smerzi. Optimal measurements for simultaneous quantum estimation of multiple phases. *Phys. Rev. Lett.*, 119:130504, Sep 2017.
- [28] Jing Yang, Shengshi Pang, Yiyu Zhou, and Andrew N. Jordan. Optimal measurements for quantum multiparameter estimation with general states. *Phys. Rev. A*, 100:032104, Sep 2019.
- [29] Haidong Yuan. Sequential feedback scheme outperforms the parallel scheme for hamiltonian parameter estimation. *Phys. Rev. Lett.*, 117:160801, Oct 2016.
- [30] Le Bin Ho and Yasushi Kondo. Multiparameter quantum metrology with postselection measurements. *Journal of Mathematical Physics*, 62(1):012102, 01 2021.
- [31] Johannes Jakob Meyer, Johannes Borregaard, and Jens Eisert. A variational toolbox for quantum multi-parameter estimation. *npj Quantum Information*, 7(1):89, Jun 2021.
- [32] Huangjun Zhu. Information complementarity: A new paradigm for decoding quantum incompatibility. *Scientific Reports*, 5(1):14317, Sep 2015.
- [33] Sammy Ragy, Marcin Jarzyna, and Rafał Demkowicz-Dobrzański. Compatibility in multiparameter quantum metrology. *Phys. Rev. A*, 94:052108, Nov 2016.
- [34] G. E. Uhlenbeck and L. S. Ornstein. On the theory of the brownian motion. *Phys. Rev.*, 36:823–841, Sep 1930.
- [35] C. W. Helstrom. *Quantum Detection and Estimation Theory*. Academic Press, New York, 1976.
- [36] A.S. Holevo. *Probabilistic and Statistical Aspects of Quantum Theory*. Springer, New York, 1st edition, 2011.
- [37] Lorcán O. Conlon, Jun Suzuki, Ping Koy Lam, and Syed M. Assad. The gap persistence theorem for quantum multiparameter estimation, 2022.
- [38] Masahito Hayashi and Yingkai Ouyang. Tight cramér-rao type bounds for multiparameter quantum metrology through conic programming, 2023.
- [39] Marco G A Paris. Quantum state estimation. *International Journal of Quantum Information*, 7(1):125–137, 2009.
- [40] Lorcán O. Conlon, Jun Suzuki, Ping Koy Lam, and Syed M. Assad. Efficient computation of the nagaoka–hayashi bound for multiparameter estimation with separable measurements. *npj Quantum Information*, 7(1):110, Jul 2021.

- [41] M. Hayashi, editor. *Asymptotic Theory of Quantum Statistical Inference: Selected Papers*. World Scientific Singapore, 2005.
- [42] Steven Kay. *Estimation theory, Vol 1*. Prentice Hall, Englewood Cliffs, NJ, 1st edition, 1993.
- [43] Yuxiang Yang, Giulio Chiribella, and Masahito Hayashi. Attaining the ultimate precision limit in quantum state estimation. *Communications in Mathematical Physics*, 368(1):223–293, May 2019.
- [44] Koichi Yamagata, Akio Fujiwara, and Richard D. Gill. Quantum local asymptotic normality based on a new quantum likelihood ratio. *The Annals of Statistics*, 41(4):2197 – 2217, 2013.
- [45] Jasminder S. Sidhu, Yingkai Ouyang, Earl T. Campbell, and Pieter Kok. Tight bounds on the simultaneous estimation of incompatible parameters. *Phys. Rev. X*, 11:011028, Feb 2021.
- [46] Jamie Friel, Pantita Palittapongarnpim, Francesco Albarelli, and Animesh Datta. Attainability of the holevo-cramér-rao bound for two-qubit 3d magnetometry, 2020.
- [47] Francesco Albarelli, Jamie F. Friel, and Animesh Datta. Evaluating the holevo cramér-rao bound for multiparameter quantum metrology. *Phys. Rev. Lett.*, 123:200503, Nov 2019.
- [48] Rafał Demkowicz-Dobrzański, Wojciech Górecki, and Mădălin Guță. Multi-parameter estimation beyond quantum fisher information. *Journal of Physics A: Mathematical and Theoretical*, 53(36):363001, aug 2020.
- [49] K Matsumoto. A new approach to the cramér-rao-type bound of the pure-state model. *Journal of Physics A: Mathematical and General*, 35(13):3111, mar 2002.
- [50] Peter C. Humphreys, Marco Barbieri, Animesh Datta, and Ian A. Walmsley. Quantum enhanced multiple phase estimation. *Phys. Rev. Lett.*, 111:070403, Aug 2013.
- [51] Nathan Shettell and Damian Markham. Graph states as a resource for quantum metrology. *Phys. Rev. Lett.*, 124:110502, Mar 2020.
- [52] Yunkai Wang and Kejie Fang. Continuous-variable graph states for quantum metrology. *Phys. Rev. A*, 102:052601, Nov 2020.
- [53] Lorenzo Maccone and Alberto Ricciardi. Squeezing metrology: a unified framework. *Quantum*, 4:292, July 2020.
- [54] Manuel Gessner, Augusto Smerzi, and Luca Pezzè. Multiparameter squeezing for optimal quantum enhancements in sensor networks. *Nature Communications*, 11(1):3817, Jul 2020.
- [55] G. Carrara, M. G. Genoni, S. Cialdi, M. G. A. Paris, and S. Olivares. Squeezing as a resource to counteract phase diffusion in optical phase estimation. *Phys. Rev. A*, 102:062610, Dec 2020.
- [56] Klaus Mølmer and Anders Sørensen. Multiparticle entanglement of hot trapped ions. *Phys. Rev. Lett.*, 82:1835–1838, Mar 1999.
- [57] Bálint Koczor, Suguru Endo, Tyson Jones, Yuichiro Matsuzaki, and Simon C Benjamin. Variational-state quantum metrology. *New Journal of Physics*, 22(8):083038, aug 2020.
- [58] Keras. Earlystopping callback - keras documentation. https://keras.io/api/callbacks/early_stopping/, 2021. [Online; accessed 28-March-2023].
- [59] Mihai D. Vidrighin, Gaia Donati, Marco G. Genoni, Xian-Min Jin, W. Steven Kolthammer, M. S. Kim, Animesh Datta, Marco Barbieri, and Ian A. Walmsley. Joint estimation of phase and phase diffusion for quantum metrology. *Nature Communications*, 5(1):3532, Apr 2014.
- [60] Samson Wang, Enrico Fontana, M. Cerezo, Kunal Sharma, Akira Sone, Lukasz Cincio, and Patrick J. Coles. Noise-induced barren plateaus in variational quantum algorithms. *Nature Communications*, 12(1):6961, Nov 2021.
- [61] M. Cerezo, Andrew Arrasmith, Ryan Babbush, Simon C. Benjamin, Suguru Endo, Keisuke Fujii, Jarrod R. McClean, Kosuke Mitarai, Xiao Yuan, Lukasz Cincio, and Patrick J. Coles. Variational quantum algorithms. *Nature Reviews Physics*, 3(9):625–644, Sep 2021.
- [62] Ting Yu and J.H. Eberly. Entanglement evolution in a non-markovian environment. *Optics Communications*, 283(5):676–680, 2010. Quo vadis Quantum Optics?
- [63] Anian Altherr and Yuxiang Yang. Quantum metrology for non-markovian processes. *Phys. Rev. Lett.*, 127:060501, Aug 2021.
- [64] Jacob L. Beckey, N. Gigena, Patrick J. Coles, and M. Cerezo. Computable and operationally meaningful multipartite entanglement measures. *Phys. Rev. Lett.*, 127:140501, Sep 2021.
- [65] M Enríquez, I Wintrowicz, and K Życzkowski. Maximally entangled multipartite states: A brief survey. *Journal of Physics: Conference Series*, 698(1):012003, mar 2016.
- [66] Alice R. Cullen and Pieter Kok. Calculating concentratable entanglement in graph states. *Phys. Rev. A*, 106:042411, Oct 2022.
- [67] M. Oszmaniec, R. Augusiak, C. Gogolin, J. Kołodyński, A. Acín, and M. Lewenstein. Random bosonic states for robust quantum metrology. *Phys. Rev. X*, 6:041044, Dec 2016.
- [68] Daniel Braun, Gerardo Adesso, Fabio Benatti, Roberto Floreanini, Ugo Marzolino, Morgan W. Mitchell, and Stefano Pirandola. Quantum-enhanced measurements without entanglement. *Rev. Mod. Phys.*, 90:035006, Sep 2018.
- [69] Todd Tilma, Shinichiro Hamaji, W. J. Munro, and Kae Nemoto. Entanglement is not a critical resource for quantum metrology. *Phys. Rev. A*, 81:022108, Feb 2010.
- [70] Diederik P Kingma and Jimmy Ba. Adam: A method for stochastic optimization. In *Proceedings of the 3rd International Conference on Learning Representations (ICLR)*, 2015.
- [71] K. Mitarai, M. Negoro, M. Kitagawa, and K. Fujii. Quantum circuit learning. *Phys. Rev. A*, 98:032309, Sep 2018.
- [72] Maria Schuld, Ville Bergholm, Christian Gogolin, Josh Izaac, and Nathan Killoran. Evaluating analytic gradients on quantum hardware. *Phys. Rev. A*, 99:032331, Mar 2019.
- [73] Qiskit. Aer provider tutorial. 2021.
- [74] Dominik Šafránek. Simple expression for the quantum fisher information matrix. *Phys. Rev. A*, 97:042322, Apr 2018.
- [75] Nguyen Tan Viet, Nguyen Thi Chuong, Vu Thi Ngoc Huyen, and Le Bin Ho. tqix.pis: A toolbox for quantum dynamics simulation of spin ensembles in dicke basis. *Computer Physics Communications*, 286:108686, 2023.
- [76] Le Bin Ho, Kieu Quang Tuan, and Hung Q. Nguyen. tqix: A toolbox for quantum in x: X: Quantum measurement, quantum tomography, quantum metrology, and others. *Computer Physics Communications*, 263:107902, 2021.